Journal of Molecular Spectroscopy 257 (2009) 74–81

Contents lists available at ScienceDirect

Journal of Molecular Spectroscopy

journal homepage: www.elsevier.com/locate/jms

# Analysis of the FTIR spectrum of pyrazine using evolutionary algorithms

Michael Schmitt [a,*], Lars Biemann [a], W. Leo Meerts [b], Karl Kleinermanns [a]

[a] Heinrich-Heine-Universität, Institut für Physikalische Chemie I, Universitätsstraße 26.43.02, D-40225 Düsseldorf, Germany
[b] Molecular and Biophysics Group, Institute for Molecules and Materials, Radboud University Nijmegen, NL-6500 GL Nijmegen, The Netherlands

ARTICLE INFO

*Article history:*
Received 26 May 2009
In revised form 22 June 2009
Available online 1 July 2009

*Keywords:*
Pyrazine
Infrared spectroscopy
Evolutionary algorithms
*Ab initio* calculations

ABSTRACT

The FTIR spectrum of pyrazine in the gas phase has been measured and analyzed using automated evolutionary algorithms. For the stronger bands, the rotational constants for ground and vibrationally excited states, the correct band types and in some cases centrifugal distortion constants could be extracted. Several hot hands have been identified and assigned by comparison to a cubic force field calculation at the MP2/6-311G(d,p) level of theory. Vibrationally averaged rotational constants for the excited bands can give a further guidance in the assignment of the vibrational bands.



## 1. Introduction

Rovibrational or rovibronic spectra of medium size molecules contain a plethora of information which can be extracted using automated assignment techniques based on evolutionary algorithms (EA) even if no full rotational resolution can be achieved in the experiment [1]. This lack of rotational resolution might be caused by limitations of the experimental device, or by intrinsic properties of the investigated system, like e.g. for electronic excitation with a short excited state life time [2]. Vibrationally averaged rotational constants of the excited vibrational state contain information about the harmonic and cubic force field and can be used as further guidance in the assignment of the experimental spectra. Quartic centrifugal distortion constants contain information about the harmonic force field and Coriolis couplings. The band type images the direction of the change of the dipole moment and can be used e.g. to distinguish between different conformers with local vibrations and differing band types. Overtones of the bands, which might show up in the contours contain the anharmonic constants of this vibration. The $D_{2h}$ symmetry of pyrazine serves as a test case, which can easily be assigned to different band types due to its high symmetry. Vibrations of $B_{1u}$ symmetry give rise to *a*-type bands, while $B_{2u}$ vibrations are *b*-type bands and $B_{3u}$ are *c*-type bands. For the definition of the axis system, the inertial axes and the atomic numbering used in this publication refer to Fig. 1. This information, which can be extracted reliably from the rovibrational contours using evolutionary algorithm based fitting procedures, allows for the assignment of vibrational fundamentals and combination bands through symmetry and vibrationally averaged rotational constants. Pyrazine has been investigated experimentally thoroughly in the gas phase, the condensed phase and in the crystal using both infrared and Raman spectroscopy [3–6]. Califano et al. gave a rather extensive assignment of pyrazine based on vibrational contours in the infra-red spectrum [4]. Raman spectra in the molten state have been taken by Zarembowitch and Bokobza-Sebagh [7] and later by Billes et al. [5].

The most reliable calculations of vibrational frequencies of pyrazine up to now comprise anharmonic force fields using density functional theory (DFT) with the B97-1 exchange-correlation functional and a triple-$\zeta$ plus double polarization (TZ2P) basis set [8], and the calculation of the quartic force field of pyrazine in the B3LYP/6-31G(d) hybrid density-functional approximation [9].

## 2. Methods

### 2.1. Experimental procedures

The FTIR spectra of pyrazine have been recorded using a commercial Nicolet 5700 spectrometer. The sample was heated to 308, 315 and 550 K in a homebuilt vacuum absorption cell with a sample path of 10 cm, which is sealed with NaCl windows. Heating of the absorption cell was performed by means of heating resistors, that are connected directly to the window holders, in order to keep the windows at a slightly higher temperature than the cell to avoid condensation of the sample at the windows. The cell was evacuated and the spectra were taken at 2–3 mbar sample pressure. Pyrazine ($\geqslant$99%) was obtained from Sigma–Aldrich and used without further purification.

* Corresponding author. Fax: +49 211 81 15195.
*E-mail addresses:* mschmitt@uni-duesseldorf.de (M. Schmitt), leo.meerts@science.ru.nl (W.L. Meerts), kleinermanns@uni-duesseldorf.de (K. Kleinermanns).

0022-2852/$ - see front matter © 2009 Elsevier Inc. All rights reserved.
doi:10.1016/j.jms.2009.06.011

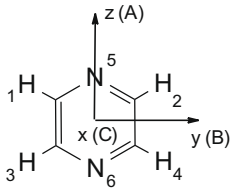


**Fig. 1.** Structure, numbering and definition of the cartesian and inertial axis system of pyrazine.

### 2.2. Computational methods

#### 2.2.1. Ab initio calculations

The structure of pyrazine in the electronic ground state has been optimized at the MP2/6-311G(d,p) level with the Gaussian 03 program package [10]. The SCF convergence criterion used throughout the calculations was an energy change below $10^{-8}$ Hartree, while the convergence criterion for the gradient optimization of the molecular geometry was $\partial E/\partial r < 1.5 \cdot 10^{-5}$ Hartree/Bohr and $\partial E/\partial \varphi < 1.5 \cdot 10^{-5}$ Hartree/degree, respectively. Harmonic frequencies have been calculated by means of analytical second derivatives of the energy with respect to the Cartesian nuclear coordinates, $\Phi_{ij}$. Anharmonic corrections to the vibrational frequencies and to the equilibrium structures were taken into account using numerical cubic ($\Phi_{ijk}$) and some of the quartic force constants ($\Phi_{ijkk}$) and computing the vibrorotational parameters using a second order perturbative approach as implemented in the Gaussian program suite [11].

#### 2.2.2. Spectral analysis using evolutionary algorithms

Evolutionary algorithms have been shown to yield reliable results for automated fits of fully rotationally resolved electronic and infrared spectra, as well as of electronic and IR band contours. Three different evolutionary algorithms were employed for the fits:

- A genetic algorithm (GA): A description of the GA used here can be found in [12,13]. The genetic algorithm is basically a global optimizer, which uses concepts copied from natural reproduction and selection processes. For a detailed description of the GA the reader is referred to the original literature [14–16].
- The derandomized-ES DR2 algorithm: The DR2 evolution strategy [17] is aimed to accumulate information about the correlation or anti-correlation of past mutation vectors in order to adapt the step size.
- The CMA evolution strategy: The CMA-ES (Covariance Matrix Adaptation Evolution Strategy) is an evolutionary algorithm for difficult non-linear non-convex optimization problems in continuous domain. It turns out to be a particularly reliable and highly competitive evolutionary algorithm for local optimization [18] and, surprising at first sight, also for global optimization [19].

All three methods use the same cost function ($C_{fg}$), which is defined as $C_{fg} = (1 - F_{fg})$ [13], where $F_{fg}$ is the fitness function:

$$F_{fg} = \frac{\sum_{r=-l}^{l} w(r) \sum_{i=1}^{N} f(i) g(i+r)}{\sqrt{\sum_{r=-l}^{l} w(r) \sum_{i=1}^{N} f(i) f(i+r)} \sqrt{\sum_{r=-l}^{l} w(r) \sum_{i=1}^{N} g(i) g(i+r)}}. \tag{1}$$

In this equation $f$ and $g$ represent the experimental and calculated spectra, respectively. The overlap function $w(r)$ determines the steepness of the error landscape.

For an asymmetric rotor spectrum of a transition between the two vibrational states, the following Hamiltonian was employed [20].

$$H_R = AJ_a^2 + BJ_b^2 + CJ_c^2. \tag{2}$$

Here $J_g (g = a, b, c)$ are the components of the body fixed angular momentum operator, $A, B$ and $C$ are the three rotational constants.

Centrifugal distortion constants may be included if necessary through the model of a distortable rotor in Watson's $A$-reduced form [21,22].

## 3. Results and discussion

Fig. 2 shows an overview of the gas phase FTIR spectrum of pyrazine at a temperature of 308 K. The fit of the individual rovibrational bands requires the consideration of nuclear spin statistics. The 144 spin functions of the two pairs of identical hydrogen atoms and one pair of identical nitrogen atoms transform like $51A_g + 27B_{2u} + 39B_{3u} + 27B_{1g}$ under the symmetry operations of

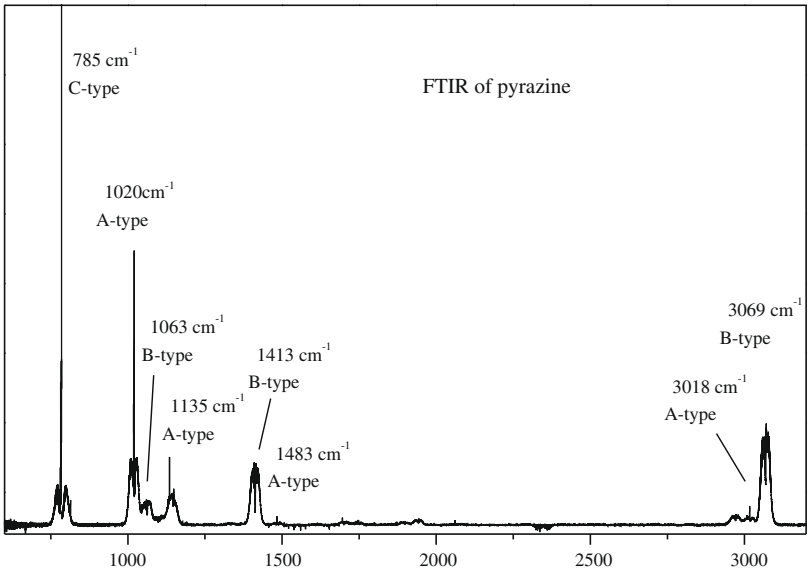


**Fig. 2.** Overview FTIR spectrum of pyrazine. Frequencies and band types of the fundamentals are given in the figure.

the point group $D_{2h}$. The 78 *gerade* spin functions combine with the *eo* and *oe* rotational states, while the 66 *ungerade* states combine with the *oo* and *ee* rotational states, where *e* and *o* designate the even and oddness of the $K_a$ and $K_c$ levels.

In the following we will present the different strategies to fit the rovibrational contours of the individual vibrational bands. For each band type one example will be shown in detail. First we will start with the *b*-type bands in the spectrum. The band at 1413 $cm^{-1}$ is shown in Fig. 3. Trace a shows the experimental spectrum.

The strongly overlapping rovibrational transitions generate a dense "background", which does not contain usable information about the spectrum, but on the other hand contributes strongly to the cost function of the evolutionary optimizer. Therefore, a direct fit of this band converges only very slowly if at all. Trace b of Fig. 3 shows the "background" of the spectrum, which has been obtained by averaging over 150 data points (1.5 $cm^{-1}$). In trace c this background is subtracted from the original spectrum. The remaining spectrum contains all the extractable information from the spectrum and can be simulated using the best parameters from an EA-fit given in Table 1. The band type of the spectrum was fitted by allowing the angles $\theta$ and $\phi$ to adapt values between 0° and 90°. For a pure *b*-type band both angles are exactly 90°. The fit ran to values above 89°. The calculated rovibrational transitions are convoluted with a Gaussian profile of 0.14 $cm^{-1}$ to take account of the experimental resolution of the spectrometer. This simulation is shown in trace d. The last trace (e) gives then the simulated spectrum after addition of the previously subtracted background. Due to the high temperature and the good signal to noise ratio for this band even the five quartic centrifugal distortion constants in the ground and vibrationally excited state could be determined. All molecular parameters are compared to the results of the anharmonic MP2/6-311G(d,p) calculation in Table 1. Very good agreement is obtained for the vibrationally averaged rotational constants for the vibrational ground state (averaged over the zero-point vibrations). Also the changes of the rotational constants upon vibrational excitation of this special mode are reproduced with a fair accuracy. The order of magnitude of the five centrifugal distortion constants from Watson's *A*-reduced Hamiltonian [21,22] $\Delta_J$, $\Delta_{JK}$, $\Delta_K$, $\delta_J$ and $\delta_K$ are correctly reproduced by the theory despite $\delta_K$ which is off by about an order of magnitude.

The same strategy was employed for the *b*-type band at 3070 $cm^{-1}$. The fit of this contour resulted in a considerably worse agreement between experiment and simulation than for the 1413 $cm^{-1}$ band. Subtracting simulation and experiment resulted in a remaining weaker component, shifted by −1.413 $cm^{-1}$, which was then included in a subsequent fit. Table 1 gives the molecular parameters of both components of this band. The existence of a second, overlapping band is in agreement with high resolution infrared, optothermal spectroscopy using a color-center laser for IR generation [23]. Due to the strongly overlapping second component it was not possible in this case to fit the centrifugal distortion constants. After the successful fit, we performed a global fit of the bands in the region between 2900 and 3100 $cm^{-1}$, which are slightly overlapping, keeping the previously determined parameters of the 3070 $cm^{-1}$ band fixed. Four bands have been identified, with center frequencies of 2971, 3007, 3018 and 3069 $cm^{-1}$. The third is an *a*-type band, the other three are *b*-type transitions.

A slightly different procedure is applied for fitting the vibrational band at 785 $cm^{-1}$. From the appearance it is clear that this band is a *c*-type band. The central *Q*-branch shows a noticeable shading to the red which cannot be explained by structure due to a single *Q*-branch, cf. Fig. 4. Instead the observed structure is due the occurrence of hot sequence bands of this vibration. Fig. 4 shows the central part of the spectrum taken at temperatures of 315 and 550 K, respectively. We added three more bands to the fit described above and fitted also the frequency separation, which reflects the difference in the $1 \leftarrow 0$, $2 \leftarrow 1$, $3 \leftarrow 2$ and $4 \leftarrow 3$ transitions. They are separated by −0.61, −1.22 and −1.89 $cm^{-1}$, respectively. The anharmonic MP2/6-311G(d,p) calculations (cf. Table 3) locate vibration 16 at 788.15 $cm^{-1}$ and the first overtone of this vibration at 1575.72 $cm^{-1}$ yielding a difference between $1 \leftarrow 0$ and $2 \leftarrow 1$ of −0.59 $cm^{-1}$ in excellent agreement with the experimental value of −0.61 $cm^{-1}$. A fourth *Q*-branch band can be observed at 781.99 $cm^{-1}$. This band is too far away to be explained by another member of the same sequence. Instead, this band can be assigned to a hot band transition originating from mode 2 which will be discussed in more detail below.

In *c*-type spectra, the overwhelmingly strong *Q*-branch poses a problem with the cost function of the EA. Since it contains nearly no structure due to the limited resolution, its appearance is com-

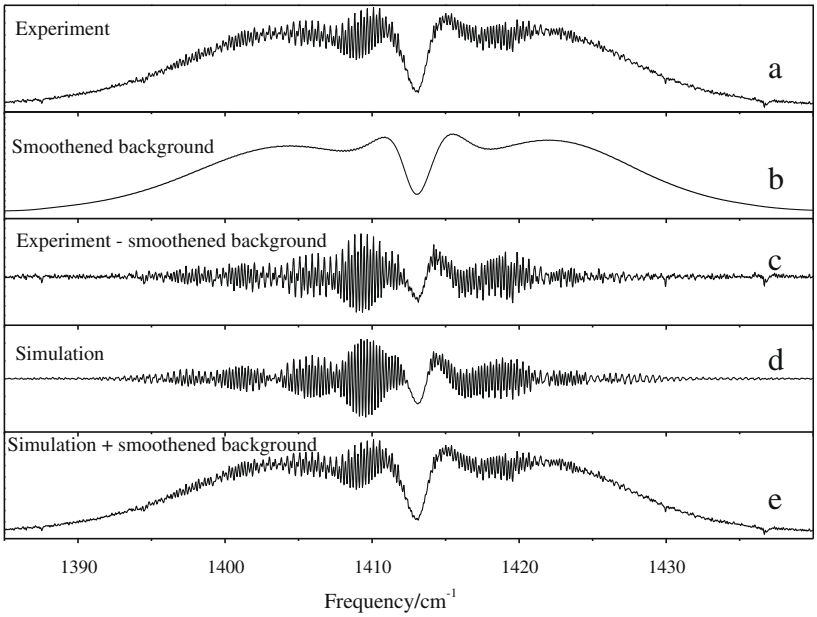


**Fig. 3.** FTIR spectrum of the 1413 $cm^{-1}$ band of pyrazine along with the best fit. For details see text.

**Table 1**
Optimized parameters from EA fits of the *b*-type rovibrational bands of pyrazine. For assignments and symmetry cf. Table 3.

| | 1413 | | 3070 | | |
|---|---|---|---|---|---|
| | Exp. | MP2 | Exp | | MP2 |
| | | | Band I | Band II | |
| Assignment | 17 | | 23 | – | 23 |
| $A/cm^{-1}$ | 0.213828(12) | 0.2139610 | 0.213823(80) | 0.213823(80) | 0.2139610 |
| $B/cm^{-1}$ | 0.197308(13) | 0.1951885 | 0.197304(87) | 0.197304(87) | 0.1951885 |
| $C/cm^{-1}$ | 0.102611(11) | 0.1020720 | 0.102608(72) | 0.102608(72) | 0.1020720 |
| $\Delta_J/10^{-6}$ cm$^{-1}$ | 0.051(7) | 0.026 | – | – | – |
| $\Delta_{JK}/10^{-6}$ cm$^{-1}$ | −0.044(21) | −0.025 | – | – | – |
| $\Delta_K/10^{-6}$ cm$^{-1}$ | 0.023(17) | 0.049 | – | – | – |
| $\delta_J/10^{-6}$ cm$^{-1}$ | −0.010(40) | 0.011 | – | – | – |
| $\delta_K/10^{-6}$ cm$^{-1}$ | 0.0018(66) | 0.017 | – | – | – |
| $\Delta I$/amu Å$^2$ | 0.01 | 0.04 | 0.0128 | 0.01 | 0.04 |
| $\nu_0/cm^{-1}$ | 1413.10 | 1413.0 | 3069.08 | 3067.67 | 3092.7 |
| $\Delta A/10^{-3}$ cm$^{-1}$ | −0.0156(15) | 0.014 | −0.22(6) | −0.21(12) | −0.152 |
| $\Delta B/10^{-3}$ cm$^{-1}$ | −0.1084(108) | −0.19 | −0.21(6) | −0.44(12) | −0.05 |
| $\Delta C/10^{-3}$ cm$^{-1}$ | −0.1330(133) | −0.16 | −0.17(4) | −0.38(8) | −0.046 |
| $\Delta\Delta_J/10^{-6}$ cm$^{-1}$ | −0.052(5) | – | – | – | – |
| $\Delta\Delta_{JK}/10^{-6}$ cm$^{-1}$ | −0.001(22) | – | – | – | – |
| $\Delta\Delta_K/10^{-6}$ cm$^{-1}$ | −0.002(20) | – | – | – | – |
| $\Delta\Delta_J/10^{-6}$ cm$^{-1}$ | −0.004(4) | – | – | – | – |
| $\Delta\Delta_K/10^{-6}$ cm$^{-1}$ | 0.0053(89) | – | – | – | – |
| $\Delta\Delta I$/amu Å$^2$ | 0.17 | 0.23 | 0.11 | 0.3624 | 0.03 |

pletely insensitive to changes of the molecular parameters. Nevertheless, it contributes more than 90% of the intensity of this band and dominates, therefore, the cost function, which is used to evaluate the quality of the fit. Therefore, we employ a weight function, which reduces the weight of the central part of the spectrum in the evaluation of the cost function:

$$W = 1 - \sum_{i=1}^{n} A^{(i)} W^{(i)}_{\text{type}}\left(\Delta^{(i)}_w, \left(\nu - \nu^{(i)}_0\right)\right) \tag{3}$$

where $A$ is the amplitude of the weight function and $\Delta^{(i)}_w$ is its width. The weight function employed here is a square function defined as:

$$W_B(\Delta_w, \Delta\nu) = \begin{cases} 1 & \text{for } |\Delta\nu| \leqslant \frac{1}{2}\Delta_w \\ 0 & \text{otherwise.} \end{cases} \tag{4}$$

We chose the amplitude in this special case to suppress 95% of the *Q*-branch intensity and subtracted additionally the smoothened background of the spectrum as described for the 1413 cm$^{-1}$ band. Fig. 5 shows the result of the fit. The smoothening tends to broaden somewhat the narrow *Q*-branch, cf. the second trace of Fig. 5 an effect which is cancelled when computing the final simulation by re-adding the smoothened background. The best fit parameters for the strongest component of this *c*-type band are collected in Table 2.

As last example we present the fit of the band(s) at 1020 cm$^{-1}$. From the rovibrational contour it is clear that this band represents an *a*-type band. As in the case of the 785 cm$^{-1}$ band, several *Q*-branches are visible, pointing to the existence of hot bands. The band has been fit using a strategy similar to that for the

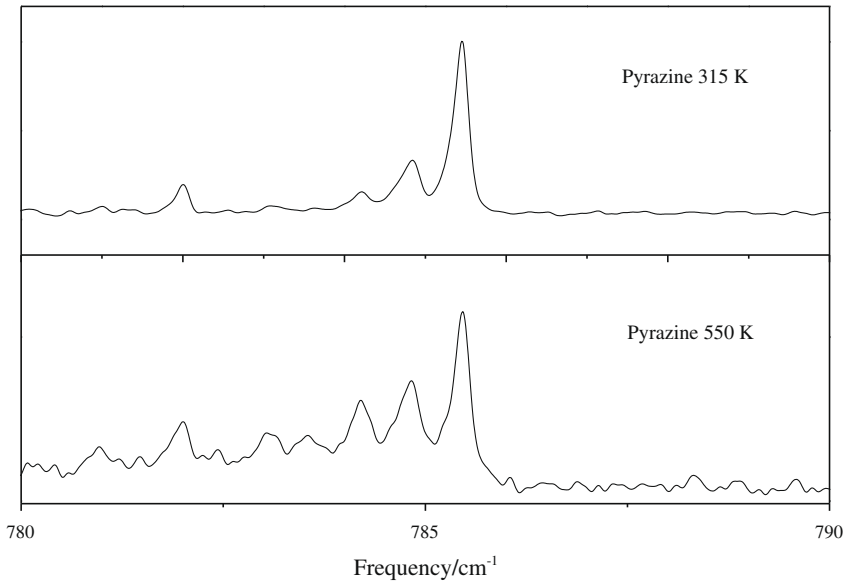


**Fig. 4.** Spectrum of the central region of the 785cm$^{-1}$ band taken at 315 and 550 K, respectively.

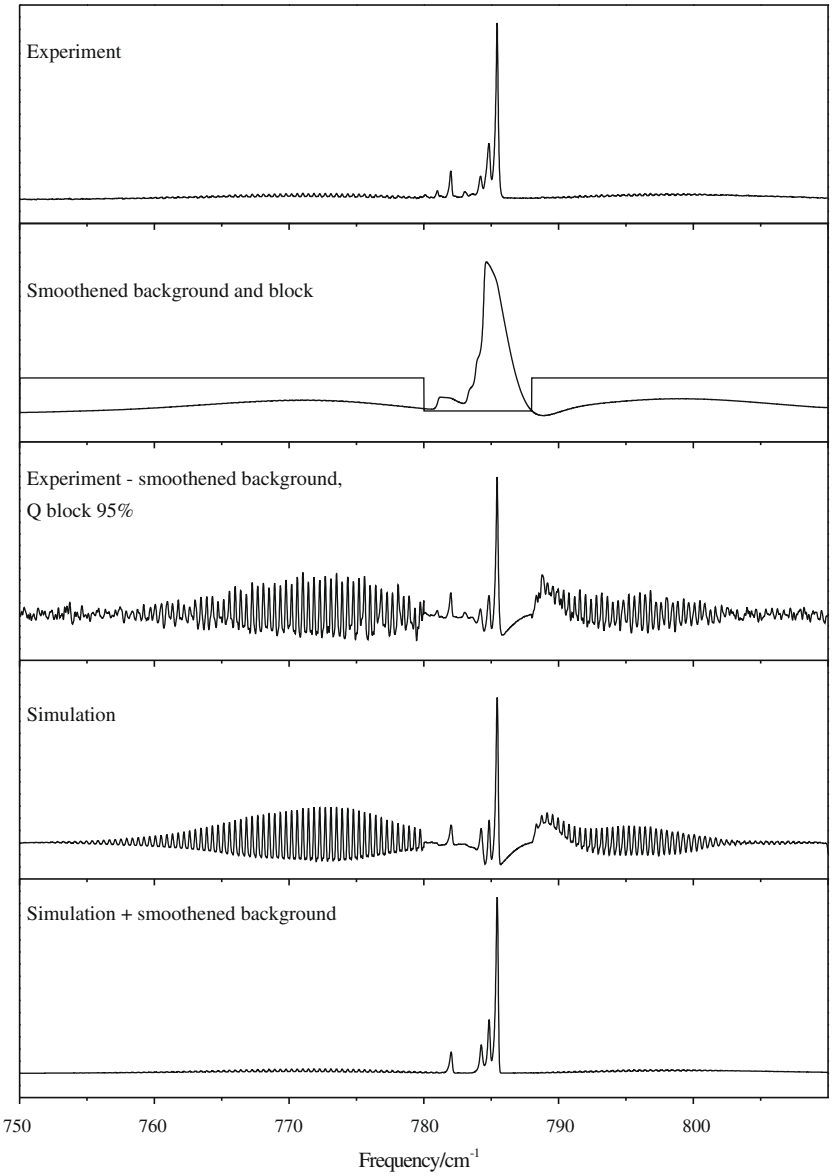


**Fig. 5.** FTIR spectrum of the 785 $cm^{-1}$ band of pyrazine along with the best fit. For details see text.

785 $cm^{-1}$ band. The intensities in the central part of the spectrum are suppressed using a 70% block filter and additionally the smoothened background is removed from the spectrum. Fig. 6 shows the results of the fit. The values of the best fit parameters for the strongest component of this band are compiled in Table 2.

For the *a*- and *c*-type bands discussed here, we compared the experimental ground state rotational constants and their changes upon vibrational excitation to the respective values of the anharmonic MP2/6-311G(d,p) calculation. For both bands good agreement for the ground state and for the vibrationally averaged

**Table 2**
Optimized parameters from EA fits of the *a*- and *c*-type rovibrational bands of pyrazine. For assignments and symmetry cf. Table 3.

| | 785 | | 1020 | |
|---|---|---|---|---|
| | Exp. | MP2 | Exp. | MP2 |
| Band type | C | | A | |
| Assignment | 6 | | 11 | |
| $A/cm^{-1}$ | 0.21382(20) | 0.2139610 | 0.21382(41) | 0.2139610 |
| $B/cm^{-1}$ | 0.19730(21) | 0.1951885 | 0.19730(26) | 0.1951885 |
| $C/cm^{-1}$ | 0.10260(38) | 0.1020720 | 0.10260(25) | 0.1020720 |
| $\Delta I$/amu Å$^2$ | 0.01 | 0.04 | 0.01 | 0.04 |
| $\nu_0/cm^{-1}$ | 785.49 | 788.1 | 1020.31 | 1019.0 |
| $\Delta A/cm^{-1}$ | −0.00022(77) | −0.000195 | 0.00008(160) | −0.000036 |
| $\Delta B/cm^{-1}$ | −0.000166(80) | −0.000163 | 0.00022(16) | 0.000250 |
| $\Delta C/cm^{-1}$ | 0.00001(5) | 0.00003 | −0.00034(11) | −0.000186 |
| $\Delta\Delta I$/amu Å$^2$ | −0.16 | −0.15 | 0.69 | 0.45 |

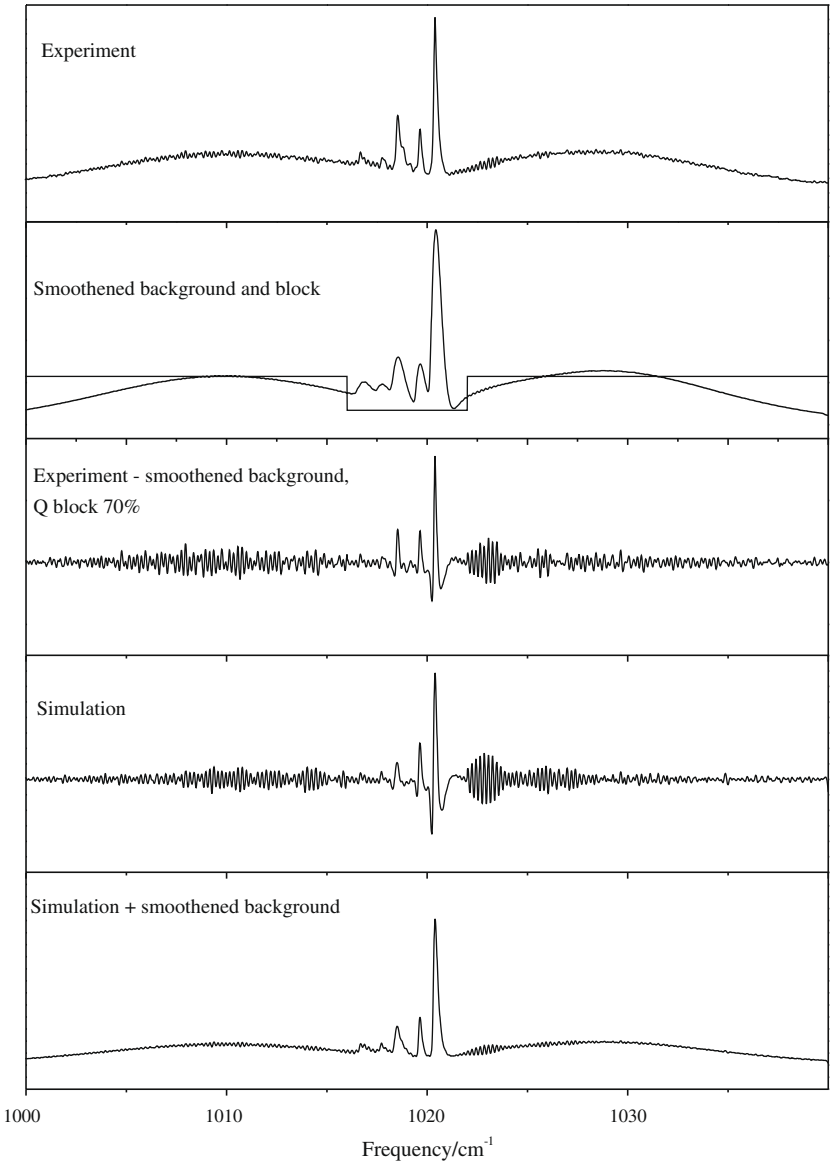


**Fig. 6.** FTIR spectrum of the 1020 $cm^{-1}$ band of pyrazine along with the best fit. For details see text.

bands is obtained. Sign as well as order of magnitude of the changes of the rotational constants are correctly predicted at this level of theory.

For the weaker vibrational bands the fit of the rotational constants yields no reliable results due to the bad signal/noise. Nevertheless, using the ground state rotational constants from the fits of the stronger bands, the band type can unequivocally be determined. Using this symmetry information and comparison to the results of the anharmonic MP2/6-311G(d,p) frequencies and their respective symmetries, all IR active fundamentals could be assigned (cf. Table 3 for harmonic and anharmonic frequencies) with the exception of the mode 15 ($B_{2u}$). The dipole moment change of this band is very close to zero and the calculated IR intensity smaller than 0.003 km/mol. This mode was previously assigned to an IR band at 1130 $cm^{-1}$ [7] or at 1335 $cm^{-1}$ [5]. Nevertheless, the anharmonically corrected frequency of 1292 $cm^{-1}$ (cf. Table 3) seems to be too far away for these assignments.

The band type, along with the vibrational frequency hence allows for the assignment of the combination bands and hot vibrational bands too, cf. Table 4. In this table, the symmetry of the combination band which is deduced from the band type of the fundamentals, as well as the assignments for the bands composing the combination and their respective symmetries are given. The hot band, which appears in the spectrum of the 785 $cm^{-1}$ band at 782 $cm^{-1}$ as a *c*-type band can be explained e.g. by the hot transition $2+6 \leftarrow 2$ (which is $\nu_{16b}(B_{3u}) + \nu_{11}(B_{3u}) \leftarrow (\nu_{16b}(B_{3u})$ in Wilson's numbering scheme). Another *c* type band at 814 $cm^{-1}$, which appears in the *R*-branch of the 785 $cm^{-1}$ band is assigned to the transition $3+10 \leftarrow 6$ in very good agreement to the calculated anharmonic frequencies in Table 4. Thus, the band type assures the assignments, which otherwise would only be based on the frequency information. The last column gives the anharmonically corrected frequency of the combination bands or of the hot vibrational bands. For the gas phase IR spectra, comprising the $B_{1u}$, $B_{2u}$ and $B_{3u}$ bands the agreement with the anharmonic frequencies is spectacular. The agreement with the Raman active $A_g$, $B_{1g}$, $B_{2g}$ and $B_{3g}$ bands, which have been measured in the liquid phase is still very good. Larger disagreement is only found for the region of the CH stretch vibrations (up to 2%).

The anharmonic force field calculations indicate two Fermi resonances in the region of the CH stretching vibrations: mode 23 at 3069.1 $cm^{-1}$ ($B_{2u}$) is resonant to the combination of modes 17 at 1413.1 $cm^{-1}$ ($B_{2u}$) and 20 at 1580 $cm^{-1}$ ($A_g$) and mode 22 at 3018.0 $cm^{-1}$ ($B_{1u}$) with the combination band of mode 18 at

**Table 3**
Harmonic ($\nu^h$) and anharmonic ($\nu^a$) normal mode frequencies (in cm$^{-1}$) and IR intensities (in km/mole) of pyrazine from the MP2/6-311G(d,p) optimized structure. The first column gives the mode index, numbered by ascending frequencies, the next column the mode assignment following the nomenclature of Wilson [24], the third column the assignment according to Mulliken [25].

| Vibration | Wilson | Mulliken | Symmetry | Band type | IR int. | $\nu^h$ | $\nu^a$ | Obs. |
|---|---|---|---|---|---|---|---|---|
| 1 | 16a | 7 | $A_u$ | – | 0.0 | 338.2 | 336.7 | 336[b] |
| 2 | 16b | 24 | $B_{3u}$ | C | 22.1 | 416.2 | 410.1 | 418[a] |
| 3 | 6a | 5 | $A_g$ | – | 0.0 | 598.7 | 589.5 | 602[a] |
| 4 | 6b | 22 | $B_{3g}$ | – | 0.0 | 710.7 | 703.3 | 704[a] |
| 5 | 4 | 14 | $B_{2g}$ | – | 0.0 | 751.0 | 747.7 | 756[a] |
| 6 | 11 | 23 | $B_{3u}$ | C | 31.0 | 798.4 | 788.1 | 785.1 |
| 7 | 10a | 8 | $B_{1g}$ | – | 0.0 | 939.2 | 925.6 | 927[a] |
| 8 | 17a | 6 | $A_u$ | – | 0.0 | 960.6 | 977.7 | 971[b] |
| 9 | 5 | 13 | $B_{2g}$ | – | 0.0 | 962.4 | 960.6 | 960[a] |
| 10 | 1 | 4 | $A_g$ | – | 0.0 | 1028.6 | 1011.7 | 1016[a] |
| 11 | 12 | 12 | $B_{1u}$ | A | 35.5 | 1035.7 | 1019.0 | 1020.3 |
| 12 | 15 | 18 | $B_{2u}$ | B | 10.0 | 1087.6 | 1060.3 | 1062.9 |
| 13 | 18a | 11 | $B_{1u}$ | A | 4.6 | 1162.4 | 1133.8 | 1135.2 |
| 14 | 9a | 3 | $A_g$ | – | 0.0 | 1257.1 | 1235.8 | 1233[a] |
| 15 | 14 | 17 | $B_{2u}$ | B | 0.0 | 1346.1 | 1292.4 | – |
| 16 | 3 | 21 | $B_{3g}$ | – | 0.0 | 1368.1 | 1339.8 | 1346[a] |
| 17 | 19b | 16 | $B_{2u}$ | B | 32.1 | 1442.2 | 1413.0 | 1413.1 |
| 18 | 19a | 10 | $B_{1u}$ | A | 2.2 | 1504.3 | 1472.7 | 1483.5 |
| 19 | 8b | 20 | $B_{3g}$ | – | 0.0 | 1563.8 | 1521.8 | 1525[a] |
| 20 | 8a | 2 | $A_g$ | – | 0.0 | 1617.0 | 1566.9 | 1580[a] |
| 21 | 7b | 19 | $B_{3g}$ | – | 0.0 | 3201.0 | 3093.4 | 3040[a] |
| 22 | 13 | 9 | $B_{1u}$ | A | 3.8 | 3201.5 | 3085.8 | 3018.0 |
| 23 | 20b | 15 | $B_{2u}$ | B | 51.4 | 3216.6 | 3092.7 | 3069.1 |
| 24 | 2 | 1 | $A_g$ | – | 0.0 | 3221.3 | 3050.0 | 3055[a] |

[a] Raman frequencies for the $A_g$, $B_{1g}$, $B_{2g}$, and $B_{3g}$ modes are taken from Ref. [7].
[b] $A_u$ modes are neither IR nor Raman active. The values given here are deduced from combination bands in Table 4.

1483.5 cm$^{-1}$ ($B_{1u}$) and mode 20 at 1580 cm$^{-1}$ ($A_g$) readily explaining the observed deviations of the vibrational frequencies in the region of the CH stretch vibrations.

## 4. Conclusions and outlook

A fit of rovibrational contours in the FTIR spectrum of pyrazine could be performed, aided by automated fits using evolutionary algorithms. Albeit the experimental resolution is limited, it is possible to extract a multitude of molecular parameters, upon them the rotational constants in both states, the absolute value of the angle of the dipole moment changes with the inertial axes, and in favorable cases even centrifugal distortion constants. Using classical (manual) line assignment based fits this task would be impossible due to the highly congested nature of these spectra.

In the present case we have only pure *a*-, *b*- and *c*-type bands due to the high symmetry of the pyrazine molecule. Nevertheless, we fit the angles $\theta$ and $\phi$, which describe the dipole moment changes for each vibration in order to test the sensitivity of the fit for the determination of the band type. In all cases, not only the correct band type was found, but also the hybrid character due to the other two orientations was always less the 1%. Thus, we are confident, that this method can be applied to molecules with less symmetry, in order to determine the relative band types in hybrid bands.

**Table 4**
Experimental vibrational frequencies, band types and assignments of all observed bands of pyrazine along with the anharmonically corrected vibrational frequencies ($\nu^a$) from the MP2/6-311G(d,p) calculations. The column "Mode" refers to the numbering according to ascending frequencies, the following columns give the assignments according to Refs. [24] and [25].

| Obs. | Type | Sym. | Mode | Wilson | Mulliken | $\nu^a$ |
|---|---|---|---|---|---|---|
| 781 | *C* | $B_{3u}$ | $[6+6]-6$ | $[6(B_{3u})+6(B_{3u})]-6(B_{3u})$ | $[23+23]-23$ | 787.7 |
| 782 | *C* | $B_{3u}$ | $[2+6]-2$ | $[16b(B_{3u})+11(B_{3u})]-16b(B_{3u})$ | $[24+23]-24$ | 788.3 |
| 785 | *C* | $B_{3u}$ | 6 | $11(B_{3u})$ | 23 | 788.1 |
| 814 | *C* | $B_{3u}$ | $[3+10]-6$ | $[6a(A_g)+1(A_g)]-11(B_{3u})$ | $[5+4]-23$ | 818.8 |
| 1020 | *A* | $B_{1u}$ | 11 | $12(B_{1u})$ | 12 | 1019.0 |
| 1063 | *B* | $B_{2u}$ | 12 | $15(B_{2u})$ | 18 | 1060.3 |
| 1099 | *B* | $B_{2u}$ | $[1+5]$ | $16a(A_u)+4(B_{2g})$ | $7+14$ | 1092.0 |
| 1135 | *A* | $B_{1u}$ | 13 | $18a(B_{1u})$ | 11 | 1133.8 |
| 1334 | *B* | $B_{2u}$ | $[2+7]$ | $16b(B_{3u})+10a(B_{1g})$ | $24+8$ | 1338.7 |
| 1413 | *B* | $B_{2u}$ | 17 | $19b(B_{2u})$ | 16 | 1413.1 |
| 1483 | *A* | $B_{1u}$ | 18 | $19a(B_{1u})$ | 10 | 1472.7 |
| 1702 | *B* | $B_{2u}$ | $[6+7]$ | $11(B_{3u})+10a(B_{1g})$ | $[23+8]$ | 1712.2 |
| 1748 | *A* | $B_{1u}$ | $[12+4]$ | $6b(B_{3g})+15(B_{2u})$ | $[18+22]$ | 1769.8 |
| 1871 | *C* | $B_{3u}$ | $[1+19]$ | $8b(B_{3g})+16a(A_u)$ | $[7+20]$ | 1857.9 |
| 1898 | *A* | $B_{1u}$ | $[7+8]$ | $10a(B_{1g})+17a(A_u)$ | $[8+6]$ | 1905.7 |
| 1943 | *B* | $B_{2u}$ | $[8+9]$ | $17a(A_u)+5(B_{2g})$ | $[6+13]$ | 1952.4 |
| 2061 | *A* | $B_{1u}$ | $[18+3]$ | $6a(A_g)+19a(B_{1u})$ | $[10+5]$ | 2060.4 |
| 2971 | *B* | $B_{2u}$ | $[17+20]$ | $19b(B_{2u})+8a(A_g)$ | $[16+2]$ | 2962.1 |
| 3007 | *B* | $B_{2u}$ | $[18+19]$ | $19a(B_{1u})+8b(B_{3g})$ | $[10+20]$ | 2986.4 |
| 3018 | *A* | $B_{1u}$ | 22 | $13(B_{1u})$ | 9 | 3085.8 |
| 3069 | *B* | $B_{2u}$ | 23 | $20b(B_{2u})$ | 15 | 3092.7 |

This procedure will be especially beneficial in cases, where local vibrations can be assigned, and the direction of the change of their dipole moment gives direct structural information about the geometric orientation of the vibrating group in the inertial frame of the molecule. Possible applications range from local N—H or C═O stretching vibrations of amino acids which appear quite isolated in their respective spectral range to artificially localized C–D stretch vibrations in singly deuterated compounds.

## Acknowledgments

This work was supported by Deutsche Forschungsgemeinschaft through Project KI531/27. The authors like to thank the National Computer Facilities of the Netherlands Organization of Scientific Research (NWO) for a grant on the Dutch supercomputing facility SARA. Granted computing time from the RRZ Köln is gratefully acknowledged. This work is part of the doctoral thesis of Lars Biemann.

## References

[1] W.L. Meerts, M. Schmitt, Int. Rev. Phys. Chem. 25 (2006) 353–406.
[2] Y. Lee, B. Kim, M. Schmitt, K. Kleinermanns, J. Phys. Chem. A 110 (2006) 11819–11823.
[3] R.C. Lord, A.L. Marston, F.A. Miller, Spectrochimica Acta 9 (1957) 113–125.
[4] S. Califano, G. Adembri, G. Sbrana, Spectrochimica Acta 20 (1964) 385–396.
[5] F. Billes, H. Mikosch, S. Holly, J. Mol. Struct. Theochem 423 (1998) 225–234.
[6] S. Breda, I. Reva, L. Lapinski, M. Nowak, R. Fausto, J. Mol. Struct. 786 (2006) 193–206.
[7] J. Zarembowitch, L. Bokobza-Sebagh, Spectrochimica Acta A 32 (1976) 605–615.
[8] A.D. Boese, J.M.L. Martin, J. Phys. Chem. A 108 (2004) 3085–3096.
[9] K.V. Berezin, V.V. Nechaev, P.M. El'kin, J. Appl. Spectrosc. 72 (2005) 9–19.
[10] M.J. Frisch, G.W. Trucks, H.B. Schlegel, G.E. Scuseria, M.A. Robb, J.R. Cheeseman, J.A. Montgomery, Jr., T. Vreven, K.N. Kudin, J.C. Burant, J.M. Millam, S.S. Iyengar, J. Tomasi, V. Barone, B. Mennucci, M. Cossi, G. Scalmani, N. Rega, G.A. Petersson, H. Nakatsuji, M. Hada, M. Ehara, K. Toyota, R. Fukuda, J. Hasegawa, M. Ishida, T. Nakajima, Y. Honda, O. Kitao, H. Nakai, M. Klene, X. Li, J.E. Knox, H.P. Hratchian, J.B. Cross, V. Bakken, C. Adamo, J. Jaramillo, R. Gomperts, R.E. Stratmann, O. Yazyev, A.J. Austin, R. Cammi, C. Pomelli, J.W. Ochterski, P.Y. Ayala, K. Morokuma, G.A. Voth, P. Salvador, J.J. Dannenberg, V.G. Zakrzewski, S. Dapprich, A.D. Daniels, M.C. Strain, O. Farkas, D.K. Malick, A.D. Rabuck, K. Raghavachari, J.B. Foresman, J.V. Ortiz, Q. Cui, A.G. Baboul, S. Clifford, J. Cioslowski, B.B. Stefanov, G. Liu, A. Liashenko, P. Piskorz, I. Komaromi, R.L. Martin, D.J. Fox, T. Keith, M.A. Al-Laham, C.Y. Peng, A. Nanayakkara, M. Challacombe, P.M.W. Gill, B. Johnson, W. Chen, M.W. Wong, C. Gonzalez, J.A. Pople, Gaussian 03, Revision C.02, Gaussian, Inc., Wallingford, CT, 2004.
[11] V. Barone, J. Chem. Phys. 122 (2005) 014108-1–014108-10.
[12] J.A. Hageman, R. Wehrens, R. de Gelder, W.L. Meerts, L.M.C. Buydens, J. Chem. Phys. 113 (2000) 7955–7962.
[13] W.L. Meerts, M. Schmitt, G. Groenenboom, Can. J. Chem. 82 (2004) 804–819.
[14] J.H. Holland, Adaption in Natural and Artificial Systems, The University of Michigan Press, Ann-Arbor, MI, 1975.
[15] D.E. Goldberg, Genetic Algorithms in search, optimisation and machine learning, Addison–Wesley, Reading, MA, 1989.
[16] I. Rechenberg, Evolutionsstrategie – Optimierung technischer Systeme nach Prinzipien der biologischen Evolution, Frommann-Holzboog, Stuttgart, 1973.
[17] A. Ostenmeier, A. Gawelcyk, N. Hansen, Step-size adaptation based on non-local use of selection information, in: Y. Davidor, H.-P. Schwefel, R. Männer (Eds.), Parallel Problem Solving from Nature, PPSN III, Springer, Berlin/Heidelberg, 1994.
[18] N. Hansen, A. Ostermeier, Evol. Comput. 9 (2) (2001) 159–195.
[19] N. Hansen, S. Kern, Evaluating the CMA evolution strategy on multimodal test functions, in: X. Yao et al. (Eds.), Parallel Problem Solving from Nature PPSN VIII, vol. 3242 of LNCS, Springer, Berlin/Heidelberg, 2004, pp. 282–291.
[20] H.C. Allen, P.C. Cross, Molecular Vib-Rotors, Wiley, New York, 1963.
[21] J.K.G. Watson, J. Chem. Phys. 46 (1967) 1935.
[22] J.K.G. Watson, J. Chem. Phys. 48 (1968) 4517.
[23] K.B. Hewett, M. Shen, C.L. Brummel, L.A. Philips, J. Chem. Phys. 100 (1994) 4077–4086.
[24] E.B. Wilson, Phys. Rev. 45 (1934) 706.
[25] R.S. Mulliken, J. Chem. Phys. 23 (1955) 1997–2011.